Engineering photon cascades from multiexciton complexes in a self-assembled quantum dot by a lateral electric field

Marek Korkusinski,[1] Michael E. Reimer,[2] Robin L. Williams,[2] and Pawel Hawrylak[1]
[1]*Quantum Theory Group, Institute for Microstructural Sciences, National Research Council, Ottawa, Canada K1A0R6*
[2]*Quantum Physics Group, Institute for Microstructural Sciences, National Research Council, Ottawa, Canada K1A0R6*
(Received 17 October 2008; published 9 January 2009)

We demonstrate theoretically that by applying an in-plane electric field it is possible to engineer and tune photon cascades originating from recombination of multiexciton complexes confined in self-assembled quantum dots. We find the multiexciton energies and states as functions of the field using the effective-mass configuration-interaction approach with the effects of electron-hole exchange treated perturbatively, and use Fermi's golden rule to compute the emission spectra. We show that the field-induced Stark shift of the energies of photons emitted by the biexciton and two linearly polarized excitons is strongly renormalized by the electron-hole interactions, which are governed by the separation of electrons and holes induced by the field. As a result, the effective Stark shifts of exciton and biexciton emission lines have opposite signs, leading to a removal of the biexciton binding energy at a finite field. This enables the cascade of a pair of polarization entangled photons in the presence of a finite exciton anisotropic exchange splitting. We compare these emission spectra to those of the charged exciton, the triplet biexciton, and the three-exciton complex. We find that the electric field and Coulomb interactions differentiate the biexciton-exciton cascade from other cascades, facilitating identification of its spectra and practical implementation.

DOI: 10.1103/PhysRevB.79.035309 PACS number(s): 78.67.Hc

I. INTRODUCTION

There is currently a great deal of interest in using self-assembled quantum dots (SADs) as optically active media for generation of single photons,[1–7] entangled photon pairs,[1,8–10] quantum repeaters,[11] and in optic-based quantum computing.[12–14] The SADs are quasi-two-dimensional structures which strongly confine both electrons and holes in the growth direction. The lateral confinement, on the other hand, is typically softer, resulting in atomiclike single-particle energy shells.[15–17] Application of a vertical electric field allows one to control the single-dot properties, such as the total charge[18] and the field-induced Stark shift,[19,20] as well as the tunneling in vertically coupled double quantum-dot molecules.[21–25] However, only a lateral electric field allows one to tune and engineer the properties of quantum dots related to their shell structure and Coulomb interactions. It has been shown that the lateral field allows one to tune the fine structure of the excitonic emission spectrum,[26–28] the efficiency of the radiative recombination of carriers, and the total confined charge[29] while modifying the interplay of the single-particle confinement and interaction effects to produce the anomalous excitonic Stark effect.[30–32] The splitting of the excitonic emission spectrum due to the anisotropic exchange interaction is an important impediment to the generation of entangled photon pairs from the biexciton-exciton cascade.[2,8,9,26,27]

Here we show that the lateral electric field can be used to control the multiexciton photon cascade in a single SAD. We focus on the biexciton-exciton cascade and show that this allows a source of entangled photon pairs to be engineered even for anisotropic dots with two linearly polarized excitonic emission states. To demonstrate this, we approximate the SAD confinement for electrons and holes with a two-dimensional parabolic confinement and compute the energies and states of the multiexcitons using the configuration-interaction approach with the electron-hole exchange effects treated perturbatively. Once the many-exciton states are derived, we utilize Fermi's golden rule to calculate the emission spectra.

Application of an in-plane electric field introduces a displacement of the electronic potential with respect to that of the hole. As a result, the electron-hole interactions diminish as a consequence of the field-induced separation of charges. The reduction in electron-hole attraction introduces a blueshifting term into the energy of the exciton, which partially compensates for the Stark redshift of the single-particle electron and hole energies. This compensation is even stronger in the energy of the biexciton. In consequence, the emission spectra of two linearly polarized single excitons exhibit only a weak redshift, while the biexciton emission blueshifts with the increase in the field. At a finite field the biexciton binding energy is removed, and the emission peaks corresponding to photons emitted by the biexciton and the exciton cross even in the presence of the anisotropic exchange splitting brought about by the electron-hole exchange. This sets up a condition in which a pair of polarization entangled photons can be emitted.

As already mentioned, application of the electric field may change the charge state of the dot. Also, the field-induced separation of carriers leads to a reduction in the radiative recombination rate, which increases the probability of generation of higher-order multiexciton complexes. By comparing the emission spectra of the exciton and biexciton to those of the charged exciton, the triplet biexciton and the three-exciton complex, we show that the electric field and Coulomb interactions differentiate the biexciton-exciton cascade from other cascades. This facilitates identification of the spectra and practical implementation.

The paper is organized as follows. In Sec. II we describe the model and the computational procedure. In Sec. III we

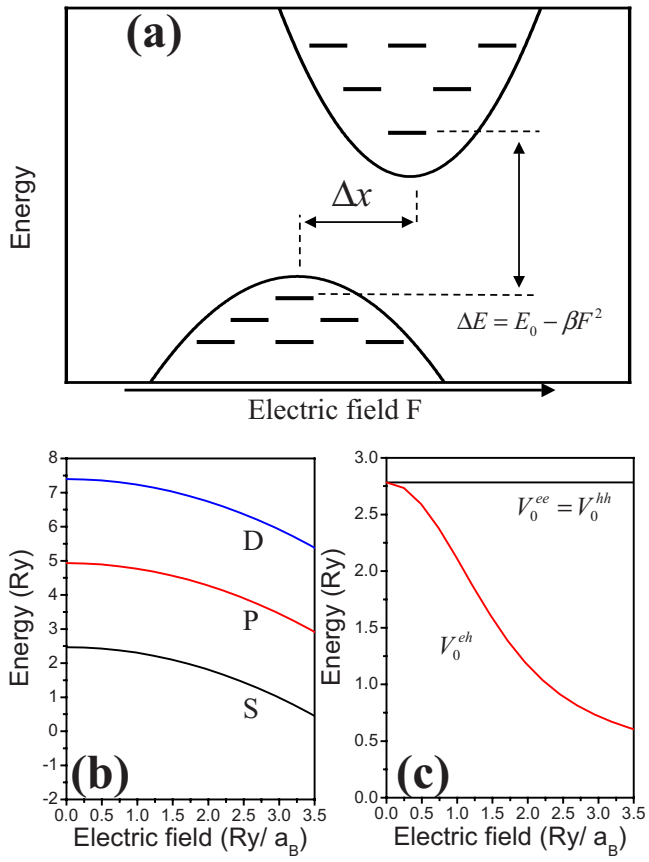

FIG. 1. (Color online) Fundamental properties of the quantum dot in a lateral electric field. (a) Schematic picture of the system. (b) Energies of the single-particle states of an electron as a function of the field. (c) Fundamental Coulomb matrix elements V_0^{ee}, V_0^{hh}, and V_0^{eh} as functions of the field.

discuss in detail the exciton and biexciton cascade as a function of the lateral electric field. In Sec. IV we present a comparison of this cascade to the emission spectra of charged excitons and other multiexciton complexes, and in Sec. V we give a summary of our results.

II. MODEL

A. Single-particle states

Recent magnetophotoluminescence experiments[17] show that the lateral confinement of the SAD can be well approximated by a two-dimensional harmonic oscillator (HO) potential. In the following we assume that this potential is acting in the x-y plane, and the external electric field $\vec{F}=F\hat{x}$ is directed along the x axis. The profile of this confinement along the field direction is shown schematically in Fig. 1(a), with the upper and lower parabolas representing the electron and hole potentials, respectively. The Hamiltonian of an electron with the effective mass m_e^* and charge $(-e)$ in such a displaced HO potential takes the form

$$\hat{H}_e = -\frac{\hbar^2}{2m_e^*}\Delta + \frac{1}{2}m_e^*\omega_e^2\left[\left(x-\frac{eF}{m_e^*\omega_e^2}\right)^2 + y^2\right] - \frac{1}{2m_e^*}\left(\frac{eF}{\omega_e}\right)^2, \tag{1}$$

where $\hbar\omega_e$ is the characteristic HO energy. The electric field displaces the origin of the potential by $x_0^e=+eF/m_e^*\omega_e^2$. The eigenstates of this Hamiltonian are the displaced HO states $|n_e,m_e,\sigma_e\rangle$, where $n_e,m_e=0,1,\ldots$ are the HO quantum numbers, and $\sigma_e=\pm 1/2$ (or $\uparrow,\downarrow$) is the electron spin. Due to the separability of Hamiltonian (1), the wave functions are simple products of one-dimensional HO states, $\langle r|n_e,m_e\rangle = \phi_{n_e}(x-x_0^e)\phi_{m_e}(y)$. The corresponding single-particle eigenenergies, $E^e(n_e,m_e)=\hbar\omega_e(n_e+m_e+1)-E_S^e$, are represented by bars within the upper parabola in Fig. 1(a). The electric field introduces a Stark shift $E_S^e=\frac{1}{2m_e^*}(\frac{eF}{\omega_e})^2$ of HO energies but without changing the energy $\hbar\omega_e$. As a consequence, for any F, the single-particle spectra consist of equally spaced shells (s, p, d, etc.) with increasing degeneracy. The shell structure is not changed by the symmetry breaking introduced by the field, a rather counterintuitive result. The electric-field dependence of the single-particle energies is plotted in Fig. 1(b).

In our treatment of holes we neglect the valence subband mixing effects and write the single-hole Hamiltonian in the form analogous to Eq. (1), only scaled with the heavy-hole effective mass m_h^* and charge $(+e)$, and the hole characteristic HO energy $\hbar\omega_h$. Due to the opposite charge, the electric field displaces the origin of the hole confinement in the direction opposite to that of the electron, $x_0^h=-eF/m_h^*\omega_h^2$. The displaced HO hole eigenstates $|n_h,m_h,\sigma_h\rangle$ are labeled by the heavy-hole spin $\sigma_h=\pm 3/2$ (or $\Uparrow,\Downarrow$), and the corresponding single-particle energies $E^h(n_h,m_h)=\hbar\omega_h(n_h+m_h+1)-E_S^h$ exhibit a Stark shift of $E_S^h=\frac{1}{2m_h^*}(\frac{eF}{\omega_h})^2$. The dependence of these energies on the electric field is qualitatively similar to that of the electrons, as shown in Fig. 1(b).

In the following we express all energies in units of the electronic effective Rydberg, $\mathcal{R}=m_e^*e^4/2\varepsilon^2\hbar^2$, and all lengths in units of the electronic effective Bohr radius, $a_B=\varepsilon\hbar^2/m_e^*e^2$, where ε is the dielectric constant of the material. With $m_e^*=0.055\ m_0$ and $\varepsilon=12.4$ we have $\mathcal{R}=4.867$ meV and $a_B=11.93$ nm. In these dimensionless units the electronic oscillator length is $\ell_e=1/\sqrt{\Omega_e}$ and the separation of the origins of the electron and hole confinements is $\Delta x=x_0^e-x_0^h = 2\frac{eF\ell_e^2 a_B}{\mathcal{R}}(\frac{1}{\Omega_e}+\frac{1}{\Omega_h})$. For our model calculations we take $\Omega_e=2.466\mathcal{R}$ (i.e., $\hbar\omega_e=\Omega_e\mathcal{R}=12$ meV) and $\Omega_h=1.233\mathcal{R}$ (i.e., $\hbar\omega_h=6$ meV), and the heavy-hole effective mass $m_h^*=0.11\ m_0$.

B. Many-body Hamiltonian

We populate the single-particle states with N_e electrons and N_h holes. Denoting the creation (annihilation) operator of an electron on state $i\equiv\{n_e,m_e,\sigma_e\}$ by c_i^+ (c_i) and the analogous pair of operators for the hole by h_i^+ (h_i), we write the Hamiltonian of the interacting electron-hole system as

$$\hat{H} = \sum_i E_i^e c_i^+ c_i + \sum_i E_i^h h_i^+ h_i + \frac{1}{2}\sum_{ijkl} \langle ij|V_{ee}|kl\rangle c_i^+ c_j^+ c_k c_l + \frac{1}{2}\sum_{ijkl} \langle ij|V_{hh}|kl\rangle h_i^+ h_j^+ h_k h_l - \sum_{ijkl} \langle ij|V_{eh}|kl\rangle c_i^+ h_j^+ h_k c_l + \hat{H}_{\mathrm{EHX}}. \quad (2)$$

The first two terms of this Hamiltonian define the single-particle energies of electrons and holes, respectively, while the third and fourth terms account for the Coulomb interactions among electrons and among holes, respectively. These terms are scaled by the Coulomb scattering matrix elements, which in the HO basis can be evaluated analytically. It is convenient to express their values in terms of the fundamental element $\langle 00|V_{ee}|00\rangle = V_0^{ee} = \sqrt{\pi\Omega_e}$. As the electric field does not change the oscillator energy $\Omega_{e(h)}$, the interactions among the carriers of the same kind do not depend upon F. The fifth term in Hamiltonian (2) accounts for the direct electron-hole interaction. Since the electric field separates electrons from holes, the matrix elements of this interaction depend upon the distance $\Delta x = x_0^e - x_0^h$. Figure 1(c) shows the dependence of the fundamental matrix elements V_0^{ee}, V_0^{hh}, and V_0^{eh} on the electric field.

The last term of Hamiltonian (2) represents the electron-hole exchange interaction. Guided by the analysis of Takagahara,[33] we account for the fact that the wave functions of the exciton and biexciton are built predominantly out of the s-shell electron and hole orbitals. As a result, we expect that the details of the fine structure of the exciton will be only weakly sensitive to the asymmetry of the SAD. Following Ref. 34, we approximate the exchange Hamiltonian $\hat{H}_{\mathrm{EHX}}$ with an effective operator in which the electron-hole exchange interaction only acts on the spins of the electron and the hole but do not redistribute carriers on single-particle orbitals. The electron-hole exchange Hamiltonian is written as

$$\hat{H}_{\mathrm{EHX}} = \sum_{ijkl} \sum_{\sigma_1^e \sigma_2^e} \sum_{\sigma_1^h \sigma_2^h} \langle i\sigma_1^e, j\sigma_1^h|V_X|k\sigma_2^h, l\sigma_2^e\rangle c_{i\sigma_1^e}^+ h_{j\sigma_1^h}^+ h_{k\sigma_2^h} c_{l\sigma_2^e}. \quad (3)$$

In our approximation we specify the elements $\langle i\sigma_1^e, j\sigma_1^h|V_X|j\sigma_2^h, i\sigma_2^e\rangle$ in the basis of spinors $\{|i\sigma^e, j\sigma^h\rangle\} = \{|i\downarrow, j\Uparrow\rangle, |i\uparrow, j\Downarrow\rangle, |i\downarrow, j\Downarrow\rangle, |i\uparrow, j\Uparrow\rangle\}$. In this basis, the matrix of Hamiltonian (3) involving the electron orbital i and the hole orbital j takes the form

$$\hat{H}_{\mathrm{EHX}}^{(ij)} = \frac{1}{2}\begin{pmatrix} \Delta_0^{(ij)} & \Delta_1^{(ij)} & 0 & 0 \\ \Delta_1^{(ij)} & \Delta_0^{(ij)} & 0 & 0 \\ 0 & 0 & -\Delta_0^{(ij)} & \Delta_2^{(ij)} \\ 0 & 0 & \Delta_2^{(ij)} & -\Delta_0^{(ij)} \end{pmatrix}. \quad (4)$$

The exchange matrix elements Δ_α^{ij} are parametrized as

$$\Delta_\alpha^{ij}(F) = \Delta_\alpha^{ij}(F=0)\frac{\int dxdy|\phi_i^e(x-x_0^e,y)|^2|\phi_j^h(x-x_0^h,y)|^2}{\int dxdy|\phi_i^e(x,y)|^2|\phi_j^h(x,y)|^2}.$$

The elements depend on the electric field through the electron and hole displacements x_0^e and x_0^h and are renormalized by the zero-field integral appearing in the denominator. We express $\Delta_\alpha^{ij}(F)$ in terms of the fundamental elements $\Delta_\alpha^{00}(F=0)$ at zero electric field. These parameters were recently estimated in high-resolution photoluminescence experiments on excitons in InAs/GaAs SADs (Ref. 34) and found to be $\Delta_0^{00}=400$ μeV, $\Delta_1^{00}=180$ μeV, and $\Delta_2^{00}=90$ μeV. Although these parameters were found to depend on the size and geometry of the SAD, we take them as model constants setting the correct energy scale of the electron-hole exchange interactions. The dependence of these fundamental exchange parameters on the electric field is computed using the displaced $|00\rangle$ electron and hole HO states as $\Delta_0^{00}(F)=\Delta_0^{00}(F=0)\exp[-(x_e-x_h)^2/4\ell^2]$. A more detailed treatment of the electron-hole exchange in the presence of the lateral electric field based on atomistic calculations will be presented elsewhere.[35]

C. Configurations and computational procedure

We look for the eigenenergies and eigenstates of the system of N_e electrons and N_h holes in the configuration interaction approach. This procedure involves creating all possible configurations of the carriers on the single-particle states, constructing the Hamiltonian matrix in the basis of these configurations for each value of the electric field and diagonalizing this matrix numerically. The computation is carried out in two steps. First, we consider Hamiltonian (2) without the electron-hole exchange term. This Hamiltonian conserves the projections S_z^e and S_z^h of the total spin of electrons and holes, respectively. This allows one to divide the configurations into subspaces labeled by the same pair (S_z^e, S_z^h) and perform the exact diagonalization in each subspace separately. In constructing the many-particle configurations we use the single-particle states of s, p, and d shells (altogether six states) for both electrons and holes. In this basis we can create, e.g., 36 configurations for an exciton, 1296 configurations for a biexciton with $S_z^e=S_z^h=0$, 225 configurations for a biexciton with $S_z^e=-1$ and $S_z^h=+3$, and 8100 configurations for $N_e=N_h=3$, $S_z^e=-1/2$ and $S_z^h=+3/2$.

In the second step we account for the electron-hole exchange interaction in an approximate manner. Because of the small energy scale for this interaction we build the matrix of the Hamiltonian $\hat{H}_{\mathrm{EHX}}$ in the basis of degenerate many-body eigenstates with the same value of total spin but all possible spin projections.

D. Emission spectra

We calculate the emission spectrum $I(\Omega)$ of the electron-hole system using Fermi's golden rule,

$$I(\Omega) = \sum_f |\langle N_e, N_h, i|\hat{P}^-|N_e - 1, N_h - 1, f\rangle|^2 \delta(E_i - E_f - \Omega). \tag{5}$$

The radiative recombination takes place from the initial state $|N_e, N_h, i\rangle$ of N_e electrons and N_h holes. The summation extends over all final states $|N_e-1, N_h-1, f\rangle$ of N_e-1 electrons and N_h-1 holes. The energy of the emitted photon equals the energy difference between the initial and final states. The amplitude of the outgoing radiation is determined from the dipole matrix element involving the interband polarization operator $\hat{P}^-$. The form of this operator depends on whether we include the above electron-hole exchange Hamiltonian in our many-body calculations. If this term is not accounted for, we take, e.g., $\hat{P}^-_+ = \Sigma_{ije}\langle i|j\rangle_h c_{i\downarrow} h_{j\Uparrow}$ in order to remove a single electron-hole pair from the system so that the outgoing photon is $\sigma+$ polarized. An analogous operator P^-_- describes the emission of the $\sigma-$ photons. On the other hand, in the presence of the electron-hole exchange a more appropriate formalism involves horizontal and vertical polarizations so that $\hat{P}^-_H = \frac{1}{\sqrt{2}}\Sigma_{ije}\langle i|j\rangle_h (c_{i\downarrow} h_{j\Uparrow} + c_{i\uparrow} h_{j\Downarrow})$. In both cases each pair of annihilation operators is scaled by the overlap ${}_e\langle m_e n_e|n_h m_h\rangle_h$ of corresponding single-particle electron and hole HO functions. For example, the overlap between the s-shell states is ${}_e\langle 00|00\rangle_h = \exp[-(\Delta x)^2/8\ell_e^2]$, while the overlap between the s-shell electron and p-shell hole states is ${}_e\langle 00|01\rangle_h = 0$ and ${}_e\langle 00|10\rangle_h = \frac{1}{2\ell_e}\Delta x \exp[-(\Delta x)^2/8\ell_e^2]$. The dependence on the electric field enters via $\Delta x = x_0^e - x_0^h$ so that as the electric field grows, the first of these elements decreases monotonically, while the last one increases and then decreases. In general, at zero electric field the only nonzero overlaps are found between the states belonging to the same shells, while at finite fields the nonzero overlaps can appear also between states originating from different shells.

III. EXCITON-BIEXCITON CASCADE IN THE PRESENCE OF THE LATERAL ELECTRIC FIELD

A. Exciton

Let us begin our discussion by summarizing the properties of the single exciton in the presence of the lateral electric field presented in detail elsewhere.[30,31] The lowest-energy configuration of the single exciton involves the two carriers occupying the respective s shells. We can generate four such configurations. One of them is $|X,a\rangle = c^+_{00\downarrow} h^+_{00\Uparrow}|0\rangle$, and the remaining three differ by the alignment of the electron and hole spins. In the absence of the electron-hole exchange these configurations have the same energy, $E_{X,a} = E^e(0,0) + E^h(0,0) - V_0^{eh}$, which is a sum of the energies of the s-shell electron and hole and their Coulomb attractions. We have already shown in Fig. 1(b) that the single-particle energies decrease quadratically with the electric field, introducing a redshift of the energy of the outgoing photon. However, as we have shown in Fig. 1(c), the electron-hole attraction V_0^{eh} also decreases with the increase in the field, resulting in a blueshift of the photon energy. This cancellation of the Stark redshift by the decrease in the exciton binding energy leads to a relatively weak dependence of the energy $E_{X,a}$ on the electric field.[30,31]

The lowest-energy excitonic configuration is the dominant component in the full exciton wave function computed in the configuration-interaction procedure. The configuration mixing effects lower the energy $E_{X,a}$ by the correlation correction ΔE_X^c, but the dependence of the exciton ground-state energy on the electric field remains qualitatively the same.

In order to account for the electron-hole exchange, we diagonalize the Hamiltonian $\hat{H}_{\mathrm{EHX}}$ given by Eq. (4) in the basis of the four s-shell exciton configurations. Based on the selection rules described in Sec. II D, among the four resulting exciton eigenstates we find two optically active ones. One of them, $|XV\rangle = \frac{1}{\sqrt{2}}(c^+_{00\downarrow} h^+_{00\Uparrow} - c^+_{00\uparrow} h^+_{00\Downarrow})|0\rangle$, with energy $E_X(V) = E_{X,a} + (\Delta_0 - \Delta_1)/2$, is vertically polarized, while the second state, $|XH\rangle = \frac{1}{\sqrt{2}}(c^+_{00\downarrow} h^+_{00\Uparrow} + c^+_{00\uparrow} h^+_{00\Downarrow})|0\rangle$, with energy $E_X(H) = E_{X,a} + (\Delta_0 + \Delta_1)/2$, is horizontally polarized. The anisotropic exchange splitting between these two states, $\Delta_{\mathrm{AEX}} = \Delta_1$, decreases with the increase in the field as derived in Sec. II B.

Note that our perturbative approach to the electron-hole exchange does not reveal any correlation between the direction of SAD anisotropy leading to the exchange splitting and the direction of the electric field. Results of more detailed atomistic calculations, accounting for the shape asymmetry and atomistic details of the SAD in relation with the field direction, will be presented elsewhere.[35]

B. Biexciton

Let us now add the second electron-hole pair to the system. The biexciton configuration with the lowest single-particle energy, $|XX,a\rangle = c^+_{00\uparrow} c^+_{00\downarrow} h^+_{00\Uparrow} h^+_{00\Downarrow}|0\rangle$, is formed when all the carriers are placed on the s-shell orbital and form spin-singlet pairs. This configuration is shown schematically in the inset of Fig. 2(a). The energy of this configuration, $E_{XX,a} = 2E_{X,a} + V_0^{ee} + V_0^{hh} - 2V_0^{eh}$, contains the energy of two noninteracting excitons $|X,a\rangle$, the electron-electron and hole-hole repulsions and twice the electron-hole attraction. If we neglect the exciton-exciton interactions (the three last terms), the biexciton energy is simply twice the energy of the exciton. In Fig. 2(a) we plot this energy as a function of the electric field with the solid red line. If we were to switch off only the electron-hole attraction (the last term in $E_{XX,a}$), the biexciton energy $E_{XX,a}$ would be given by E_{LIM}, shown in Fig. 2(a) with the blue dashed line. In the presence of all interaction terms and at zero electric field the attractive electron-hole term cancels the two repulsive Coulomb terms exactly, and the full energy $E_{XX,a}$, plotted in Fig. 2(a) with the solid blue line, is equal to $2E_{X,a}$. As the electric field increases, the attractive term decreases, resulting in an *increase* in the energy $E_{XX,a}$, which now shifts closer to its limiting value E_{LIM}. This convergence is clear in Fig. 2(a) for large values of the field. The complete biexciton energy E_{XX}, accounting for the configuration mixing in the exact diagonalization approach, is plotted in Fig. 2(a) with the black line. It is lowered from the single-configuration energy $E_{XX,a}$ by the biexciton correlation correction ΔE_{XX}^c and shows a very weak dependence on the electric field. Since this biex-

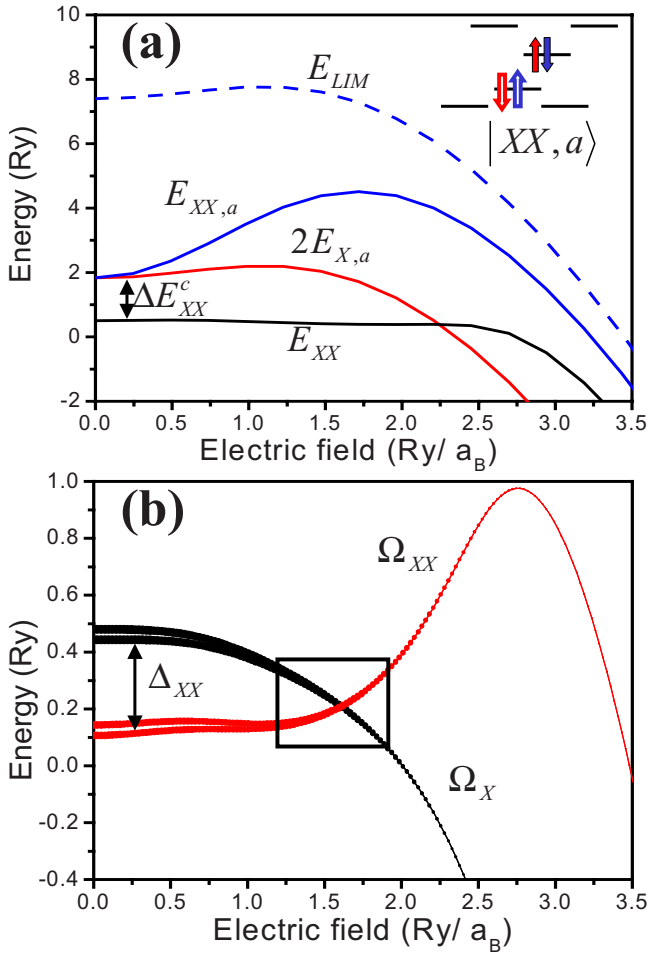

FIG. 2. (Color online) (a) Components of the biexciton ground-state energy as functions of the electric field (see text). Inset shows the lowest-energy biexciton configuration. (b) Emission spectra of the exciton (Ω_X, black) and biexciton (Ω_{XX}, red) as a function of the field. Sizes of the symbols are proportional to the emission amplitudes.

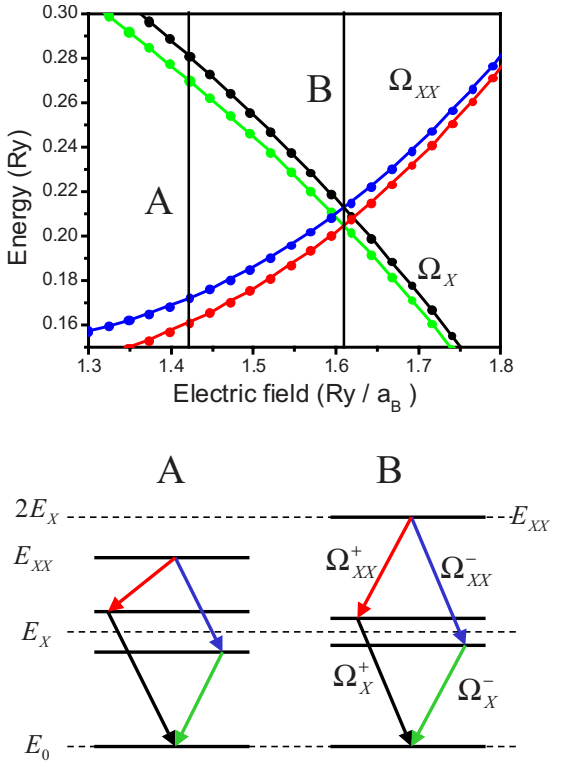

FIG. 3. (Color online) Top panel: emission spectra of the exciton (green and black) and biexciton (red and blue) in the vicinity of the $X-XX$ crossing [the region within the black rectangle in Fig. 2(b)]. Bottom panel: biexciton-exciton cascade for a small electric field (A) and at the crossing of levels (B). In the second case the energies of the transitions denoted by parallel arrows are identical, and polarization entanglement occurs.

citon state is an electron and hole singlet, its energy is not renormalized by the electron-hole exchange.

C. Biexciton-exciton cascade

Figure 2(b) shows the emission spectra of the biexciton and exciton as functions of the electric field. The exciton emission peaks, shown in black, form a doublet split by the anisotropic exchange Δ_{AEX}. The positions of these peaks correspond simply to the respective exciton energies $E_X(H)$ and $E_X(V)$.

The position of the biexciton emission peak corresponds to the energy difference $\Omega_{XX}=E_{XX}-E_X=E_{X,a}+V_0^{ee}+V_0^{hh}-2V_0^{eh}-(\Delta E^c_{XX}-\Delta E^c_X)$. We compare this energy to that of the photon emitted by the exciton $\Omega_X=E_{X,a}-\Delta E^c_X$. If we neglect the correlation effects, the cancellation of the interaction terms at zero field leads to the appearance of the exciton and biexciton peaks at the same energy. With increasing electric field, the photon emitted by the exciton redshifts while the photon from the biexciton blueshifts following the decrease in V_0^{eh} and starts to redshift only when this element is sufficiently small. When correlations in the exciton and biexciton systems are included, the biexciton photon energy Ω_{XX} is lower than the exciton photon energy Ω_X by the field-dependent biexciton binding energy Δ_{XX}. Hence, if the biexciton photon energy is reduced below the exciton photon energy by the exciton-exciton interaction, there must be a *crossing* of the exciton and biexciton emission lines for a finite electric field, as shown in Fig. 2(b).

In Fig. 2(b) the thickness of the lines corresponds to the emission amplitude. We find that for both the exciton and the biexciton this amplitude decreases with the increase in the field. This is due to the renormalization of the optical selection rules, described in Sec. II D. In both cases the emission involves a recombination of an *s*-shell electron with an *s*-shell hole, and the overlap of these two single-particle orbitals decreases as the field increases.

Figure 3(a) shows the region of fields and energies close to the crossing [indicated in Fig. 2(b) by the rectangle]. On this energy scale it is possible to discern the electron-hole exchange splitting in both the exciton and biexciton spectra. Because of the singlet nature of the biexciton, its energy is not renormalized by the electron-hole exchange, and the splitting visible in the figure is due to two polarizations of final-state excitons. The lower panel in Fig. 3 shows schematic diagrams of the biexciton-exciton cascade before

crossing (A) and at crossing (B). Each radiative transition is represented by an arrow whose color is matched to that of the respective spectral line in Fig. 3(a). We see that before the removal of the biexciton binding energy the photon pairs of the left and right cascades are different and can be distinguished. On the other hand, the two pairs of photons generated "on-resonance" cannot be energetically distinguished and would be polarization entangled, assuming that phase coherence is maintained within the emission process.[36] In the proposed scheme the two photons forming each pair are generated in sequence, with a small delay between the recombination processes. As a result, the pairs could be distinguished by a simultaneous measurement of energy and arrival time at the detector: in one cascade the low-energy photon arrives first, while in the other one the high-energy photon arrives first. However, the entanglement of the pairs can be restored to some degree by introducing appropriate delays into the optical path of each of the photons.[37,38]

IV. OTHER MULTIEXCITON COMPLEXES

A. Charged excitons

In order to observe the electric-field tuning of the biexciton emission spectrum with respect to that of the exciton, it is necessary to achieve a stable biexciton population in the SAD. In practice, however, one may have to deal with other excitonic complexes, both neutral and charged, which can obscure the desired emission spectra.

Let us begin with the analysis of the positively charged exciton X^+ whose emission spectra as a function of the electric field are shown in Fig. 4(a). Here we consider two possible configurations of the X^+ complex. The lowest-energy configuration, $|X^+S\rangle = c^+_{00\downarrow} h^+_{00\Uparrow} h^+_{00\Downarrow}|0\rangle$, is shown in the right-hand diagram of Fig. 4(a). It is a hole spin singlet and gives the largest contribution into the full correlated ground state of X^+. Another configuration, shown in the two left-hand diagrams, is a hole spin triplet $|X^+T\rangle = c^+_{00\downarrow} h^+_{01\Uparrow} h^+_{00\Uparrow}|0\rangle$. The state in which this configuration is dominant is an excited state of the X^+ complex. However, provided that the spin-flip relaxation of the hole to the ground singlet state is sufficiently slow, such a state can be detected optically.

In Fig. 4(a) we plot the emission spectrum of the two variants of X^+: that of the X^+S with the blue line and that of the X^+T with the brown lines, with the symbol sizes corresponding to the emission amplitudes. The peak positions of the exciton and biexciton are plotted with dashed lines for reference. Note that the singlet X^+ exhibits only one emission line in the considered energy range: that corresponding to the recombination of the *s*-shell electron and the *s*-shell hole, as indicated in the top right-hand diagram. The optical signature of the triplet X^+, on the other hand, consists of two lines. One of them, at lower energy, corresponds to the recombination of the *s*-shell electron with the *s*-shell hole (bottom left-hand diagram). The other one, at higher energy, involves the *s*-shell electron and the *p*-shell hole (top left-hand diagram). It acquires a sizable oscillator strength only at finite fields. This is a consequence of the electric-field tuning of the dipole matrix elements discussed in Sec. II D.

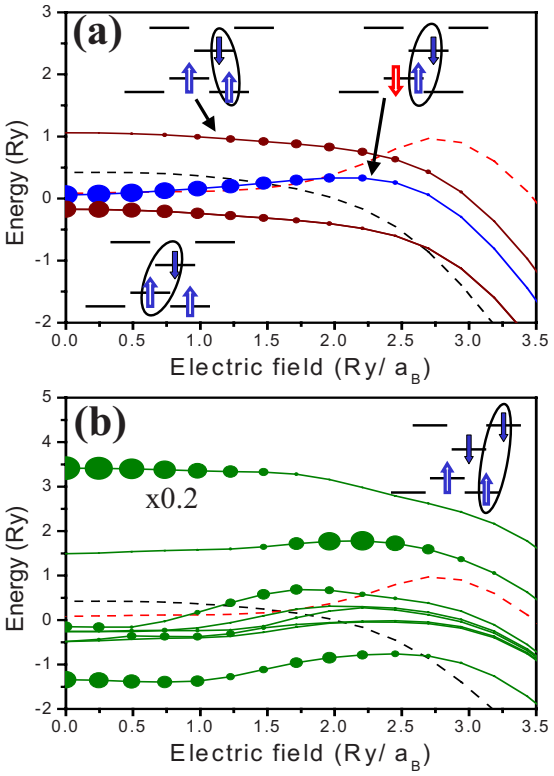

FIG. 4. (Color online) Emission spectra of (a) the positively charged exciton X^+ in a singlet and triplet hole configurations and (b) the triplet-triplet biexciton $XX-TT$ as a function of the lateral electric field. Sizes of the symbols correspond to the calculated emission amplitudes, while the black and red dashed lines indicate the positions of the exciton and biexciton peaks, respectively. Diagrams show the electron-hole configurations dominant in each of the multiexciton states.

As it can be seen in Fig. 4(a), the emission maximum of X^+S behaves similarly to that of the biexciton, both in terms of its position and amplitude. However, due to the singlet configuration of the holes, the X^+S complex does not exhibit any anisotropic exchange splitting, which makes it possible to distinguish between the two complexes. The two emission lines of X^+T exhibit the fine structure, but they can be readily identified by their monotonic redshift as a function of the field and by the fact that they appear simultaneously as a pair of lines.

B. Triplet-triplet biexciton

If both electron and hole spin-flip relaxation processes are sufficiently slow, it may be possible to observe the optical signature of the triplet-triplet biexciton whose dominant configuration, $|XX-TT\rangle = c^+_{01\downarrow} c^+_{00\downarrow} h^+_{01\Uparrow} h^+_{00\Uparrow}|0\rangle$, is shown schematically in the diagram in Fig. 4(b). In the main panel of the figure we show the emission spectra of such a complex as a function of the field, with the exciton and biexciton spectra shown with dashed lines for reference. We plot nine emission lines corresponding to nine possible configurations of the

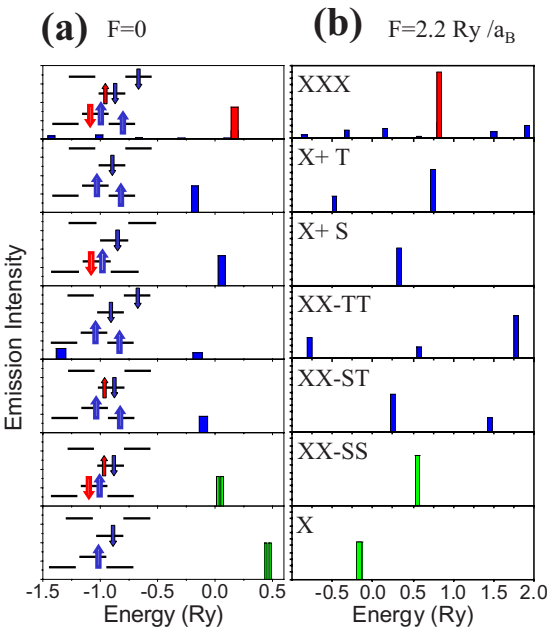

FIG. 5. (Color online) Emission spectra of neutral and charged excitonic complexes. From bottom to top: the single exciton X, the singlet-singlet biexciton $XX-SS$, the singlet-triplet biexciton $XX-ST$ with spin-polarized holes, the triplet-triplet biexciton $XX-TT$, the positively charged exciton in the hole singlet $X+S$ and hole triplet $X+T$ configurations, and the triple exciton XXX. Dominant configurations of each complex are shown schematically in diagrams. Panels (a) and (b) show the spectra at $F=0$ and $F=2.2\mathcal{R}/a_B$, respectively. Height of the bars is proportional to the calculated emission amplitude.

final-state exciton on the three electron and three hole single-particle levels. The spectrum is complicated, with the strongest line appearing at highest energies, and corresponding to the recombination of the p-shell electron and the p-shell hole. The lowest line, on the other hand, corresponds to the recombination of the s-shell exciton. The intermediate lines correspond either to the "direct" recombination of particles from the same orbitals (these lines have finite amplitude at zero field) or to the s-p recombination events (these lines become bright at finite fields). As we can see, the optical signature of $XX-TT$ is very different from that of the exciton-biexciton cascade.

C. Partially polarized biexciton and three-exciton complex

In Fig. 5 we compare the previously calculated emission spectra from the exciton-biexciton cascade, from fully spin-polarized biexciton $XX-TT$, and from the positively charged exciton in singlet (X^+S) and triplet (X^+T) hole configurations to the spectra of the partially spin-polarized biexciton $XX-ST$ and the three exciton complex XXX. We plot the emission spectra at zero electric field ($F=0$, left-hand panel) and after the biexciton-exciton crossing ($F=2.2\mathcal{R}/a_B$, right-hand panel). The corresponding dominant initial-state configurations are also shown although the $XX-SS$ state is composed of 1296 configurations and the XXX state is composed of 8100 configurations. As discussed before, at $F=0$ the exchange split exciton emission line is above the two biexciton lines, while at $F=2.2\mathcal{R}/a_B$ it is below them. The emission lines of the other five excitonic complexes are found in a similar spectral range, particularly at low fields. However, the XX-X cascade can be identified unambiguously by observing their fine structure and evolution with the electric field. As already discussed, the positively charged exciton in the singlet state X^+S (Fig. 5, third diagram from the top) exhibits no exchange splitting of its emission lines. The remaining four complexes exhibit the fine structure (not shown in Fig. 5 for clarity). However, in the three-exciton complex XXX and the triplet-triplet biexciton $XX-TT$ (first and fourth panels from the top, respectively), we deal with electron-hole pairs occupying the p shell, which results in the appearance of an additional emission maximum, located at energies by $\sim 3.7\mathcal{R}$ higher than the s-shell features (not shown). The remaining two systems, the charged exciton X^+T in the triplet state and the singlet-triplet biexciton $XX-ST$ (second and fifth panels from the top, respectively) can be identified by observing the evolution of their emission spectra with the field. At finite fields the optical selection rules permit the radiative recombination of carriers, of which one occupies the s shell, while the other occupies the p shell (such processes are forbidden at zero field). Since such pairs are found in each of these complexes, their spectra at finite fields are composed of two peaks, separated approximately by the single-particle hole energy $\hbar\omega_h$.

V. CONCLUSION

In conclusion, using the effective-mass description of single-particle electron and hole quantum-dot states and the configuration-interaction treatment of the multiexciton system, we have predicted the effective Stark shift of the photons obtained in the exciton and biexciton cascade in a lateral electric field. We have shown that this shift is a result of the interplay between the redshift of the single-particle states and the blueshifting component arising as a result of the decrease in the electron-hole attraction as the charges are being separated by the field. The correlation effect is stronger for the biexciton and results in a net blueshift of the photons due to biexciton recombination. As a result, at a finite electric field the photon emitted in exciton recombination has the same energy as that emitted in biexciton recombination. With the electron-hole exchange effects treated perturbatively we show that the anisotropic exchange splitting of the energies of photons due to exciton and biexciton decreases with the increase in the field but remains finite at the degeneracy point. However, the vertically polarized photon emitted by the biexciton is degenerate with the horizontally polarized photon emitted by the exciton at the same field as is the other pair of photons emitted with opposite polarizations. In consequence, the biexciton-exciton cascade composed of two vertically polarized photons cannot be energetically distinguished from the cascade with opposite polarizations,

making it possible to generate polarization-entangled photon pairs.

We have compared the exciton and biexciton emission spectra in the electric field with those of other multiexciton complexes likely to form in the SAD at low excitation powers. We found that the *XX*-*X* cascade exhibits a unique signature of the effective Stark shift and anisotropic exchange splitting, which allows us to distinguish it from other cascades. These properties of the *XX*-*X* cascade allow us to generate polarization-entangled photon pairs in nonconcircularly symmetric dots even in the presence of the noise due to other carriers.

ACKNOWLEDGMENTS

The authors thank Ulrich Hohenester for useful discussions and acknowledge the support of the Canadian Institute for Advanced Research, QuantumWorks, the Canadian Institute for Photonic Innovations, and the NSERC-NRC-BDC grant.

[1] A. J. Shields, Nat. Photonics **1**, 215 (2007).
[2] C. Santori, D. Fattal, J. Vuckovic, G. S. Solomon, and Y. Yamamoto, Nature (London) **419**, 594 (2002).
[3] Z. Yuan, B. E. Kardynal, R. M. Stevenson, A. J. Shields, C. J. Lobo, K. Cooper, N. S. Beattie, D. A. Ritchie, and M. Pepper, Science **295**, 102 (2002).
[4] P. Michler, A. Kiraz, C. Becher, W. V. Schoenfeld, P. M. Petroff, L. Zhang, E. Hu, and A. Imamoglu, Science **290**, 2282 (2000).
[5] J. Kim, O. Benson, H. Kan, and Y. Yamamoto, Nature (London) **397**, 500 (1999).
[6] S. Strauf, N. G. Stoltz, M. T. Rakher, L. A. Coldren, P. M. Petroff, and D. Bouwmeester, Nat. Photonics **1**, 704 (2007).
[7] M. Scholz, T. Aichele, S. Ramelow, and O. Benson, Phys. Rev. Lett. **96**, 180501 (2006).
[8] R. M. Stevenson, R. J. Young, P. Atkinson, K. Cooper, D. A. Ritchie, and A. J. Shields, Nature (London) **439**, 179 (2006).
[9] N. Akopian, N. H. Lindner, E. Poem, Y. Berlatzky, J. Avron, D. Gershoni, B. D. Gerardot, and P. M. Petroff, Phys. Rev. Lett. **96**, 130501 (2006).
[10] A. Greilich, M. Schwab, T. Berstermann, T. Auer, R. Oulton, D. R. Yakovlev, M. Bayer, V. Stavarache, D. Reuter, and A. Wieck, Phys. Rev. B **73**, 045323 (2006).
[11] H.-J. Briegel, W. Dür, J. I. Cirac, and P. Zoller, Phys. Rev. Lett. **81**, 5932 (1998).
[12] X. Li, Y. Wu, D. Steel, D. Gammon, T. H. Stievater, D. S. Katzer, D. Park, C. Piermarocchi, and L. J. Sham, Science **301**, 809 (2003).
[13] D. Bouwmeester, A. Ekert, and A. Zeilinger, *The Physics of Quantum Information* (Springer, Berlin, 2000).
[14] E. Knill, R. Laflamme, and G. J. Milburn, Nature (London) **409**, 46 (2001).
[15] P. Hawrylak and M. Korkusinski, in *Single Quantum Dots: Fundamentals, Applications, and New Concepts*, Topics in Applied Physics Vol. 90, edited by P. Michler (Springer-Verlag, Berlin, 2003).
[16] D. Gammon and D. G. Steel, Phys. Today **55** (10), 36 (2002).
[17] S. Raymond, S. Studenikin, A. Sachrajda, Z. Wasilewski, S. J. Cheng, W. Sheng, P. Hawrylak, A. Babinski, M. Potemski, G. Ortner, and M. Bayer, Phys. Rev. Lett. **92**, 187402 (2004).
[18] H. Drexler, D. Leonard, W. Hansen, J. P. Kotthaus, and P. M. Petroff, Phys. Rev. Lett. **73**, 2252 (1994).
[19] S. Raymond, J. P. Reynolds, J. L. Merz, S. Fafard, Y. Feng, and S. Charbonneau, Phys. Rev. B **58**, R13415 (1998).
[20] P. W. Fry, I. E. Itskevich, D. J. Mowbray, M. S. Skolnick, J. J. Finley, J. A. Barker, E. P. O'Reilly, L. R. Wilson, I. A. Larkin, P. A. Maksym, M. Hopkinson, M. Al-Khafaji, J. P. R. David, A. G. Cullis, G. Hill, and J. C. Clark, Phys. Rev. Lett. **84**, 733 (2000).
[21] H. J. Krenner, E. C. Clark, T. Nakaoka, M. Bichler, C. Scheurer, G. Abstreiter, and J. J. Finley, Phys. Rev. Lett. **97**, 076403 (2006).
[22] M. Scheibner, M. Yakes, A. S. Bracker, I. V. Ponomarev, M. F. Doty, C. S. Hellberg, L. J. Whitman, T. L. Reinecke, and D. Gammon, Nat. Phys. **4**, 291 (2008).
[23] G. Ortner, M. Bayer, Y. Lyanda-Geller, T. L. Reinecke, A. Kress, J. P. Reithmaier, and A. Forchel, Phys. Rev. Lett. **94**, 157401 (2005).
[24] W. Sheng and J. P. Leburton, Phys. Rev. Lett. **88**, 167401 (2002).
[25] G. Bester and A. Zunger, Phys. Rev. B **72**, 165334 (2005).
[26] K. Kowalik, O. Krebs, A. Lemaitre, S. Laurent, P. Senellart, P. Voisin, and J. A. Gaj, Appl. Phys. Lett. **86**, 041907 (2005).
[27] B. D. Gerardot, S. Seidl, P. A. Dalgarno, R. J. Warburton, D. Granados, J. M. Garcia, K. Kowalik, and O. Krebs, Appl. Phys. Lett. **90**, 041101 (2007).
[28] M. M. Vogel, S. M. Ulrich, R. Hafenbrak, P. Michler, L. Wang, A. Rastelli, and O. G. Schmidt, Appl. Phys. Lett. **91**, 051904 (2007).
[29] E. S. Moskalenko, M. Larsson, W. V. Schoenfeld, P. M. Petroff, and P. O. Holtz, Phys. Rev. B **73**, 155336 (2006).
[30] S. Ritter, P. Gartner, N. Baer, and F. Jahnke, Phys. Rev. B **76**, 165302 (2007).
[31] M. E. Reimer, M. Korkusinski, D. Dalacu, J. Lefebvre, J. Lapointe, P. J. Poole, G. C. Aers, W. R. McKinnon, P. Hawrylak, and R. L. Williams, Phys. Rev. B **78**, 195301 (2008).
[32] B. Szafran and F. M. Peeters, Phys. Rev. B **76**, 195442 (2007).
[33] T. Takagahara, Phys. Rev. B **62**, 16840 (2000).
[34] M. Bayer, G. Ortner, O. Stern, A. Kuther, A. A. Gorbunov, A. Forchel, P. Hawrylak, S. Fafard, K. Hinzer, T. L. Reinecke, S. N. Walck, J. P. Reithmaier, F. Klopf, and F. Schäfer, Phys. Rev. B **65**, 195315 (2002).
[35] M. Korkusinski, M. Zielinski, and P. Hawrylak (unpublished).
[36] F. Troiani, J. I. Perea, and C. Tejedor, Phys. Rev. B **74**, 235310 (2006).
[37] J. E. Avron, G. Bisker, D. Gershoni, N. H. Lindner, E. A. Meirom, and R. J. Warburton, Phys. Rev. Lett. **100**, 120501 (2008).
[38] G. Pfanner, M. Seliger, and U. Hohenester, arXiv:0806.0761 (unpublished).